*Conference on Modelling Fluid Flow (CMFF'22)*
*The 18th International Conference on Fluid Flow Technologies*
*Budapest, Hungary, August 30-September 2, 2022*

# EFFECT OF LEAKAGE ON THE PERFORMANCE OF THE VANELESS DIFFUSER OF A CENTRIFUGAL PUMP MODEL

Meng FAN[1], Antoine DAZIN[1], Francesco ROMANO[1], Gérard BOIS[1]

[1] Univ. Lille, CNRS, ONERA, Arts et Métiers Institute of Technology, Centrale Lille, UMR 9014-LMFL-Laboratoire de Mécanique des Fluides de Lille - Kampé de Fériet, F-59000, Lille, France

## ABSTRACT

An analysis of a pump vaneless diffuser model is presented with a particular focus on the leakage effect between the impeller outlet and diffuser inlet section. RANS and URANS simulations are conducted for three different leakage configurations. The $k-\omega$ SST turbulence model is used, carrying out the simulation by the open-source software OpenFOAM. Results obtained for each numerical configuration are analyzed and discussed. Comparison with experimental results corresponding to one of the tested configurations is also presented. They show that the leakage flow slightly influences the overall pump performance and more specifically the vaneless diffuser one. When considering the real flow rate obtained by CFD, including leakage effects, comparison with the experimental results get closer both for the overall pump and for the vaneless diffuser performances. A special focus on the instability onset in the vaneless diffuser is also proposed for each leakage configuration which leads to selecting the best way to reproduce experimental behavior from an adequate CFD approach and correct boundary conditions.

**Keywords: numerical simulation, performance, instability**

## NOMENCLATURE

| | | |
|---|---|---|
| $\delta$ | $[-]$ | relative error |
| $\Delta p$ | $[Pa]$ | pressure difference |
| $\nu_T$ | $[-]$ | eddy viscosity |
| $\omega_{imp}$ | $[rad/s]$ | angular velocity |
| $\rho$ | $[kg/m^3]$ | air density |
| $b$ | $[m]$ | diffuser width |
| $H_b$ | $[m]$ | outflow domain height |
| $L$ | $[m]$ | radial gap value |
| $N$ | $[rpm]$ | rotational speed |
| $p$ | $[Pa]$ | static pressure |
| $Q$ | $[m^3/s]$ | pump flow rate |
| $Q_d$ | $[m^3/s]$ | pump design flow rate |
| $R$ | $[m]$ | radius |
| $Re$ | $[-]$ | pump Reynolds number |
| $Z$ | $[-]$ | number of blades |

**Subscripts**

| | |
|---|---|
| 1 | impeller inlet |
| 2 | impeller outlet |
| 3 | diffuser inlet |
| 4 | diffuser outlet |
| $C$ | centrifugal pump |
| $D$ | diffuser |
| $D1$-$D9$ | related to the nine evenly distributed probes along the radial direction over the shroud side of the diffuser |
| $I$ | impeller |
| $S1$-$S4$ | related to the probes placed at $\theta = 0,\ \pi/2,\ \pi,\ 3\pi/2$ on the inlet pipe |

## 1. INTRODUCTION

Centrifugal pumps are widely used in many domains such as irrigation, water supply, cooling systems, and pumping stations. However, the operating range of pumps is affected by the occurrence of unstable phenomena. Among them, rotating stall can affect the vaneless diffuser of the pump when operating at a partial flow rate. This has been already described and analyzed by several authors in radial flow pumps and compressors like Jansen et al. [1, 2], Senoo et al. [3], Fringe et al. [4], and Sundström et al. [5]. Even if this phenomenon is now well described, the effect of the leakage flow at diffuser inlet on the rotating stall onset and dynamic has never been investigated. Detailed information on the pump model geometry can be found in Wuibaut et al. [6]. This model set-up uses air as working fluid and its dimensions are determined using similarity laws parameters, i.e same specific speed and specific radius of the initial pump working with water. To get a sufficiently high pump Reynolds number value of $Re = \omega_{imp} R^2/\nu = 5.48 \times 10^5$, based on the impeller outlet radius and a rated angular speed of $\omega_{imp} = 125$ rad/s, the air pump model's main dimensions are listed in table 1.

The present case study has been experimentally

| | |
|---|---|
| ***SHF impeller characteristics*** | |
| Tip intlet radius | $R_1 = 141.1$mm |
| Outlet radius (experiment) | $R_2 = 256.6$mm |
| Outlet radius (simulations) | $R_2 = 257.5$mm |
| Outlet width | $b_2 = 38.5$mm |
| Number of blades | $Z = 7$ |
| Outlet blade angle | $\beta_{2c}$ =22.5° |
| Design flowrate(1200 rpm) | $Q_d = 0.236\text{m}^3/\text{s}$ |
| Reynolds number | $Re = {R_2}^2\omega_{imp}/\nu$ |
| ($Q/Q_d = 1.0$, $N = 1200$ rpm) | $= 5.52\times10^5$ |
| ***Vaneless diffuser characteristics*** | |
| Inlet radius (experiment) | $R_3 = 257.1$mm |
| Inlet radius (case A) | $R_3 = 257.5$mm |
| Inlet radius (case B and C) | $R_3 = 260.075$mm |
| Outlet radius | $R_4 = 385.5$mm |
| Constant width | $b_3 = 38.5$mm |

**Table 1. Main geometrical characteristics of the impeller and diffuser**

and analytically investigated in previous works by Dazin et al. [7, 8], and by Heng et al. [9, 10] and [11], even though the effects of the leakage flow have been neglected. Some attempts to include leakage effects in CFD investigation have been presented by Dupont et al. [12] and Pavesi et al. [13] to partially explain overall mean performance discrepancies between experiments and numerical results, but with a vaned diffuser configuration. In the present paper, three different leakage configurations are numerically analyzed using RANS and URANS approaches and compared with experimental performance results on the whole pump and the vaneless diffuser itself. The limitations of the numerical methods employed on this pump model are pointed out combined with the effects of each leakage configuration.

## 2. METHODOLOGY

### 2.1. Computational Domain

The three different tested configurations are shown in figure 1. They are respectively called "case A", "case B", and "case C".

- Case A corresponds to a simplified configuration for which there is no leak between the impeller and the vaneless diffuser (see fig. 1 (a)).

- Case B corresponds to a usual pump configuration that allows leakage flow from outlet to inlet sections of the impeller. Consequently, a radial gap $L = R_3 - R_2$ is introduced as shown in fig. 1 (b).

- Case C, given in fig. 1 (c), is quite close to the experimental set-up with the same value of the radial gap value $L$. The inlet axial gap that separates the inlet tube and the rotating impeller is neglected.

The overall CFD domains include the inlet pump pipe domain (radius $R_1$ and pipe lenght $10R_1$). The outlet pump domain that is represented by an external cylinder of height $H_b$ and external radius $R_b$. An outflow box dimension of $H_b/b_3 = 15$ and outlet radius $R_b/R_3 = 3$, is placed after the diffuser outlet section.

### 2.2. Problem Formulation and Mesh

The flow in a centrifugal pump is incompressible and three-dimensional. Turbulence, rotation of the impeller, the shape of the blades, centrifugal force, and Coriolis force lead to complex flow phenomena in the centrifugal pump. In this study, the flow in the pump is described by the Reynolds averaged Navier-Stokes equations, either in steady (RANS) or unsteady (URANS) form. The URANS equations are

$$\frac{\partial(\mathbf{u})}{\partial t} + (\mathbf{u}\cdot\nabla)\mathbf{u} + \nabla p = \nabla\cdot(2\nu\mathbf{S} - \boldsymbol{\tau}), \quad \nabla\cdot\mathbf{u} = 0, \quad (1)$$

where $\mathbf{u} = \mathbf{u}(\mathbf{x}, t)$ denotes the mean part of the velocity vector, $\mathbf{u} = (u_1, u_2, u_3)$, $p = p(\mathbf{x}, t)$ denotes the mean part of the kinematic pressure, $\nu$ is the constant kinematic viscosity, $\mathbf{x}$ is the position vector, $t$ denotes time, $\mathbf{S} = \frac{1}{2}(\nabla\mathbf{u} + \nabla^T\mathbf{u})$ is the mean rate of the strain tensor with the components

$$S_{ij} = \frac{1}{2}\left(\frac{\partial u_i}{\partial x_j} + \frac{\partial u_j}{\partial x_i}\right), \quad (2)$$

and $\boldsymbol{\tau}$ is the Reynolds stress tensor.

For the (U)RANS simulation, the Reynolds stress tensor is modeled by an eddy-viscosity approach containing two conservation equations for the turbulent properties $\phi$. Depending on the model type, the placeholder $\phi$ can be the turbulent kinetic energy $k$, the turbulent dissipation $\epsilon$ or the turbulent specific dissipation rate $\omega$, respectively:

$$\frac{\partial(\phi)}{\partial t} + (\mathbf{u}\cdot\nabla)\phi = P_\phi + \nabla\cdot(D_\phi\nabla\phi) + E_\phi. \quad (3)$$

Different turbulence models contain the terms for production P, diffusion D, and dissipation E. The eddy viscosity $\nu_T$ can be deduced from the calculated turbulence quantities as $\nu_T \sim k^2/\epsilon$ or $\nu_T \sim k/\omega$ [14]. The shear-stress transport $k-\omega$ $SST$ turbulent model is used to simulate the turbulent flow in this study.

The computational mesh for the whole domain is multi-block-structured and has several refinement zones to capture the flow field in detail in areas of interest. The mesh is finest near the walls and is gradually coarser further away from the walls. The finer block-structured mesh of the short inlet pipe, impeller, and vaneless diffuser regions with a zoomed view of the refined zones in the impeller and diffuser domain is illustrated in fig. 2 (a) and fig. 2 (b). While a coarser mesh is used in the long inlet pipe and the outflow box regions. In the model scale, the numerical simulations have y+ values of approximately 1 near the walls in the short inlet pipe, impeller, and diffuser regions. The corresponding y+ value near

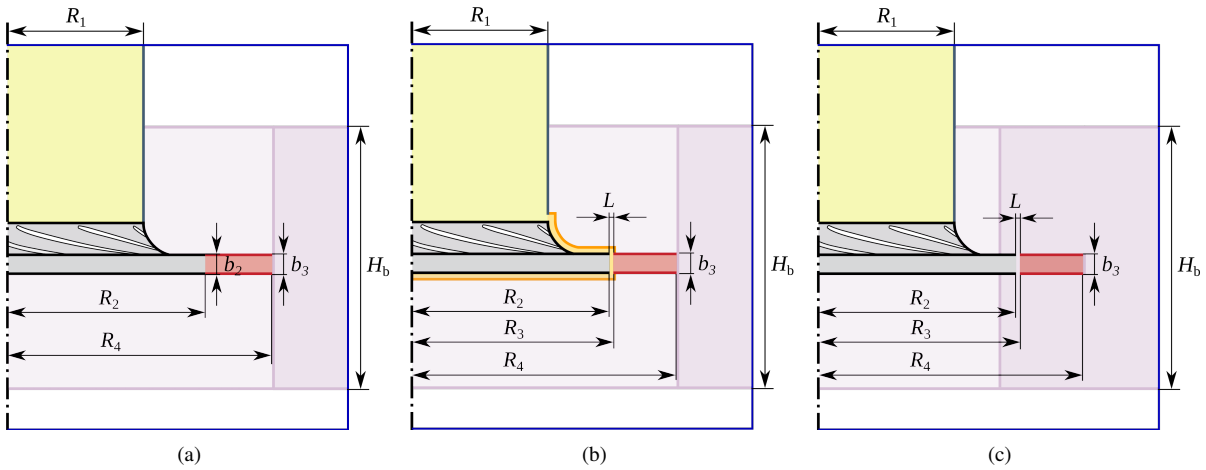


**Figure 1. Schematic of the (a) case A, (b) case B, and (c) case C of the centrifugal pump.**

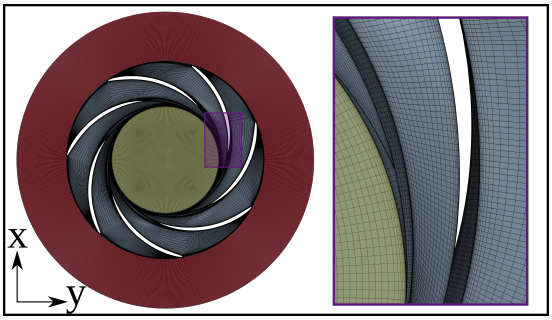


(a)

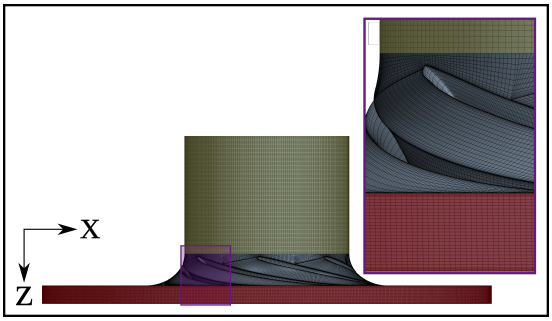


(b)

**Figure 2. Top (a) and side (b) view of a typical mesh of case A employed for carrying out the three-dimensional URANS simulations.**

the long pipe wall is less than 10 since the mesh for this region is coarser. The mesh is generated by the commercial software ANSYS ICEM CFD and then converted to the format that OpenFoam uses based on the mesh converter library `fluent3DmesToFoam`.

A grid number independence verification was carried out with four schemes. As shown in tab. 2, the predicted performance of the pump at the design condition with different grid resolutions are compared. The relative error of the predicted pump performance increases with the increase of grids sizes and then decreased to 0.93%. Therefore, a total mesh number of

| Case | Grid number | PSI | $\delta$ |
|---|---|---|---|
| 1 | 617691 | 0.3843 | 1.75% |
| 2 | 1118819 | 0.3864 | 2.30% |
| 3 | 2316400 | 0.3742 | 0.93% |
| 4 | 5406783 | 0.3777 | – |

**Table 2. Grid independence verification data. $\delta$ is the relative error computed with respect to the finest grid, i.e. $\delta = |\mathrm{PSI}_{\mathrm{Case\ 4}} - \mathrm{PSI}_{\mathrm{Case\ *}}|/|\mathrm{PSI}_{\mathrm{Case\ 4}}|$, where the asterisk denotes either Case 1, 2 or 3.**

2.3 million for the numerical domain were selected.

### 2.3. Numerics in OpenFOAM

All the numerical simulations were carried out using the open-source software OpenFOAM. The solver `simpleFoam` which enables the addition of MRF (Multiple Reference Frame) zones is applied for RANS simulations. While a transient solver `pimpleFoam` with dynamic mesh handling is applied for URANS simulations. In this simulation work, the temporal discretization term makes use of a second-order `backward` differencing scheme, named backward. The gradient term was discretized using the discretization method `Gauss` with linear interpolation where the discretization scheme is `Gauss` means gaussian interpolation of second order. The momentum divergence term was discretized using the second-order `linearUpwind` scheme, which is a blend of linear and upwind schemes. The linear scheme is used for `Interpolation` terms, where Gauss linear corrected scheme is used for Laplacian terms.

A Dirichlet type boundary condition named `flowRateInletVelocity` is chosen for the inlet boundary condition. We specify the inlet velocity corresponding to a pre-set value of inlet flow rate $Q$. And the static pressure $p = 0$ Pa is set for the outlet. The noslip wall boundary is used for fixed walls, and the `rotatingWallVelocity` boundary condi-

tion which specifies a rotational velocity is used for rotating walls.

To exclude the startup phase of the flow from the simulations, the RANS simulation results are used as initial values for URANS. The rotational speed was chosen as 125 rad/s and a time step was chosen as $\Delta t$, corresponding to 0.5° of the impeller revolution. The simulation results lead to an averaged Courant number for the whole domain of 0.0075 at the design flow rate. For RANS simulations, 10000-time steps were simulated. For URANS simulations, 70 rotating revolutions were simulated and all the results presented in this paper are corresponding to the last time step.

### 2.4. Experimental Set-ups

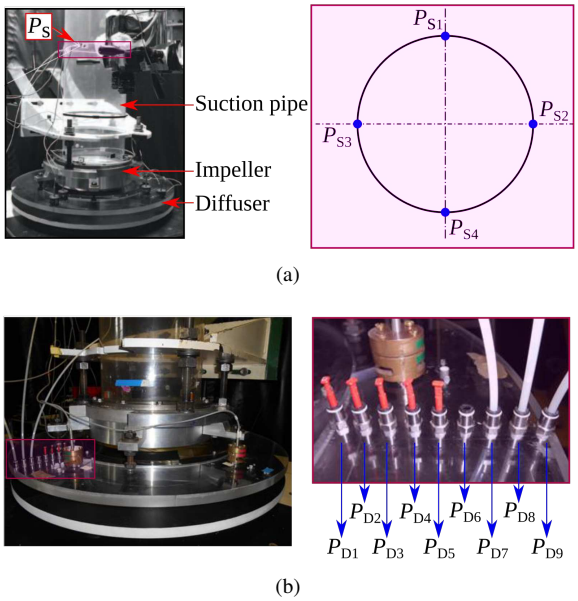


**Figure 3. (a) Static pressure taps' locations at the pump inlet pipe. (b) Wall static pressure taps and microphones' locations installed on the vaneless diffuser.**

The experimental set-up is briefly described here and is shown on fig. 3. It includes the transparent inlet pipe, the radial impeller, and the vaneless diffuser. The inlet pipe length is equivalent to the one of the numerical inlet domain. A set of replaceable diaphragms (with different inlet diameters), placed in a tank located before the inlet pipe section, are used to adjust the flow rate $Q$. No volute exists downstream the vaneless diffuser to ensure axisymmetric outlet boundary conditions corresponding to atmospheric pressure. To obtain diffuser pressure recovery, the set-up is equipped with nine steady wall pressure taps along with the diffuser shroud (equally spaced from $R$ = 264 mm to 384 mm). The corresponding measurement uncertainty is evaluated at ± 2 Pa. Several flow rates values between $Q/Q_d$ = 0.26 and 1.53 are chosen for a fixed rotational speed of $N$ = 1200 rpm. $Q_d$ denotes the design flow rate.

## 3. RESULTS

### 3.1. Pump Performance

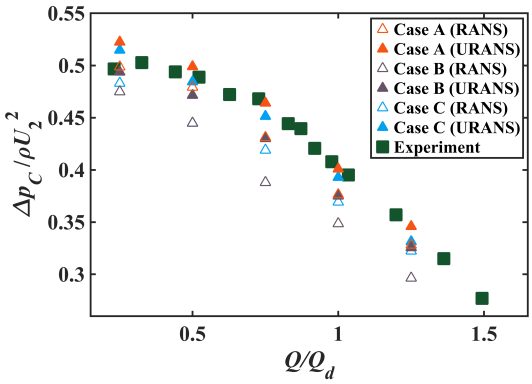


(a)

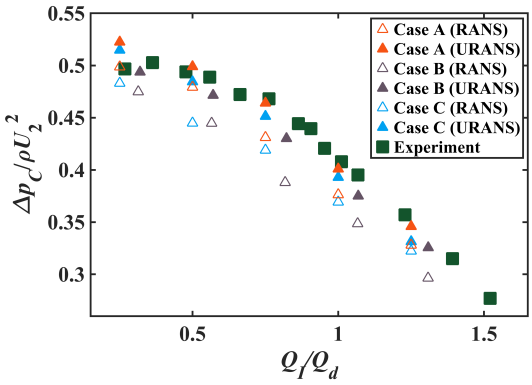


(b)

**Figure 4. (a) Overall pump performance versus reduced pump flow rate $Q$. (b) Overall pump performance versus reduced impeller flow rate $Q_I$. $\Delta p_C$ denotes the static pressure difference between the inlet and the outlet sections of the centrifugal pump; $\rho$ denotes the density of the air.**

The pump performance curves obtained by the RANS and URANS simulations are compared with the experimental results as shown in fig. 4 (a). As expected, the URANS simulation results are in better agreement with the experimental ones, as they captured the slowest scales of the time-dependent dynamics. Looking at the results of the three different configurations, the performance curve of case C, which is the same geometrical configuration as the experimental set-up, is the closest to the experimental results over the whole operating range. The performance curve of case A is slightly above the experimental results. Most of the experimental results are between the numerical results of cases A and C. Concerning case B, the pressure difference between the impeller outlet and inlet section leads to a leakage flow going out at the impeller-diffuser radial gap, feeding back the impeller inlet plane. This results in an increment of the flow rate in the impeller. Besides, an approximated flow leakage value is estimated through the inlet axial gap in front of

the impeller as already proposed by Heng [11], who modify the experimental impeller flow rate $Q_I$ which is slightly larger than $Q$. This effect is taken into account and the corrected performance curves of case C and experiment, based on the impact of the flow rate increment in the impeller, are plotted in fig. 4 (b). The corresponding simulation results of case C get closer to the experimental ones.

### 3.2. Impeller Performance

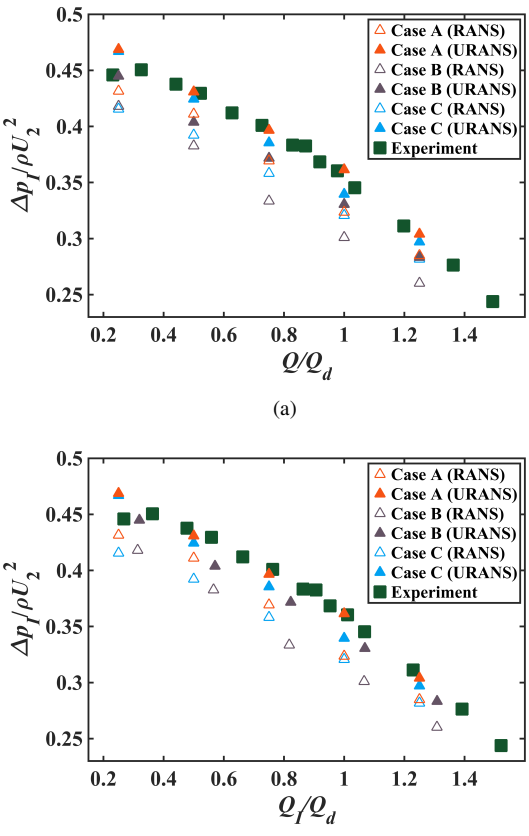


**Figure 5. (a) Impeller performance versus reduced pump flow rate $Q$. (b) Impeller performance versus the reduced impeller flow rate $Q_I$. $\Delta p_I$ denotes the static pressure difference between the inlet and the outlet impeller sections.**

Fig. 5 (a) shows the impeller performance curve obtained with the RANS and URANS approaches. The impeller performance curves are very similar to the whole pump performance curves with the same trend. However, the simulation results of the impeller performance are closer to the experimental results of the whole pump performance. This means that the pump performance is mainly dominated by the impeller performance. The shifted impeller performance curves, based on the flow rate correction method mentioned before, are shown in fig. 5 (b). The corrected results show that excepting a flow rate change, the leakage flow does not have a big impact on the impeller performances.

### 3.3. Diffuser Performance

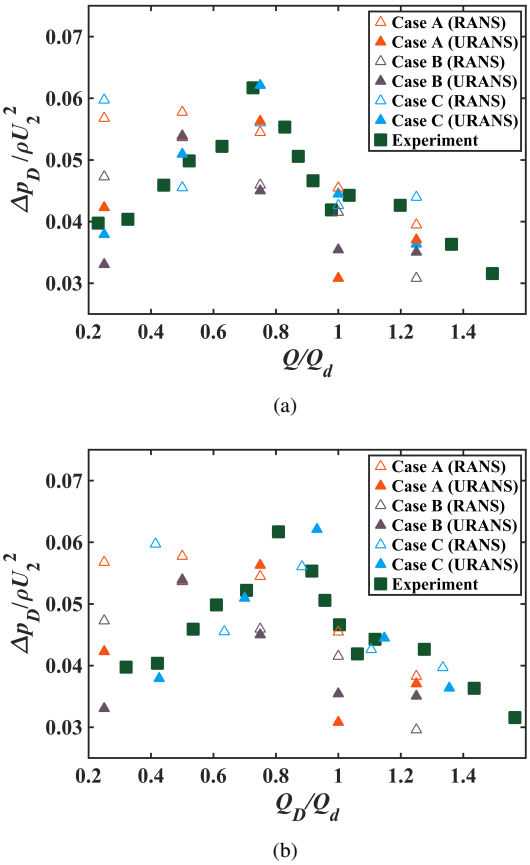


**Figure 6. (a) Diffuser pressure recovery versus reduced pump flow rate $Q$. (b) Diffuser pressure recovery versus reduced diffuser flow rate $Q_D$. $\Delta p_D$ denotes the static pressure difference between the inlet and the outlet sections of the vaneless diffuser.**

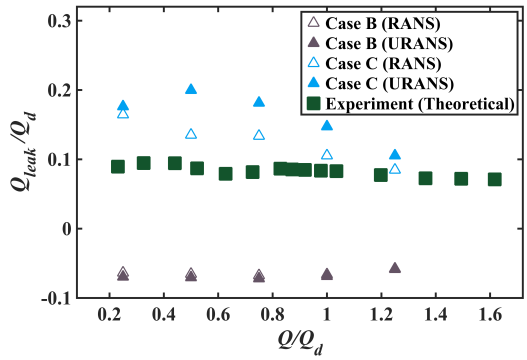


**Figure 7. Plotting of the leakage flow rates $Q_{leak}$ versus the flow rate of the pump $Q$.**

Fig. 6 (a) shows the comparison of the diffuser performance obtained by the RANS and URANS simulations for several flow rate $Q$ values. Both the RANS and URANS simulation results look acceptable under large flow rates. The real flow rate inside the diffuser $Q_D$ is higher than the flow rate $Q$ used

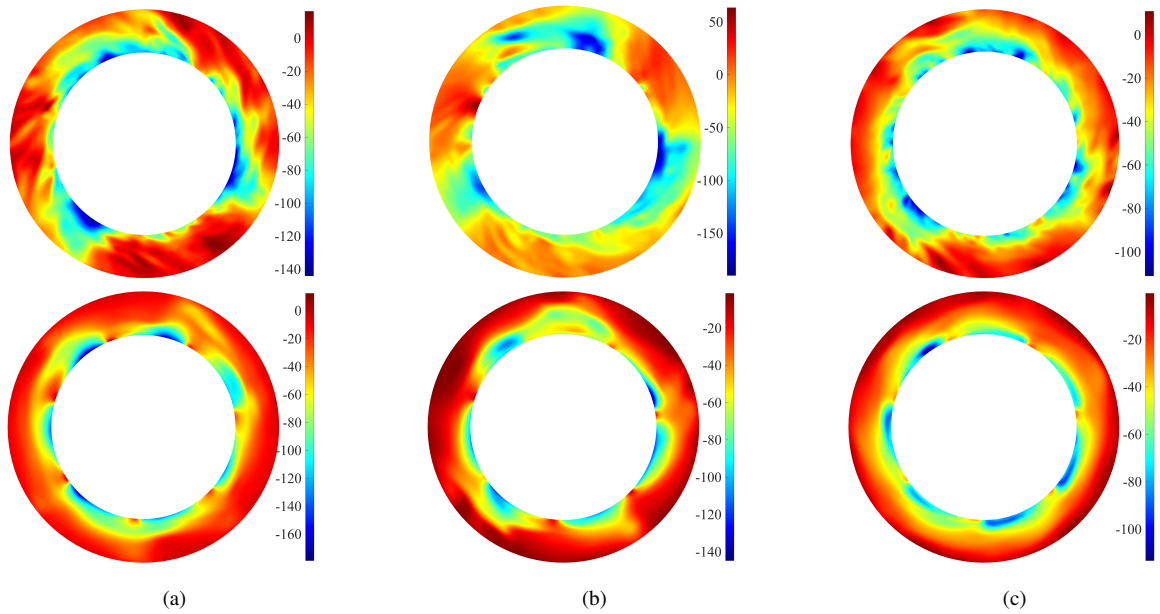


(a) (b) (c)

**Figure 8. Instantaneous color maps of the static pressure $p$ (pa) at the mid-height of the diffuser at the flow rate $Q/Q_d = 0.25$ obtained by the URANS (top figures) and RANS (bottom figures) for: (a) case A, (b) case B, and (c) case C.**

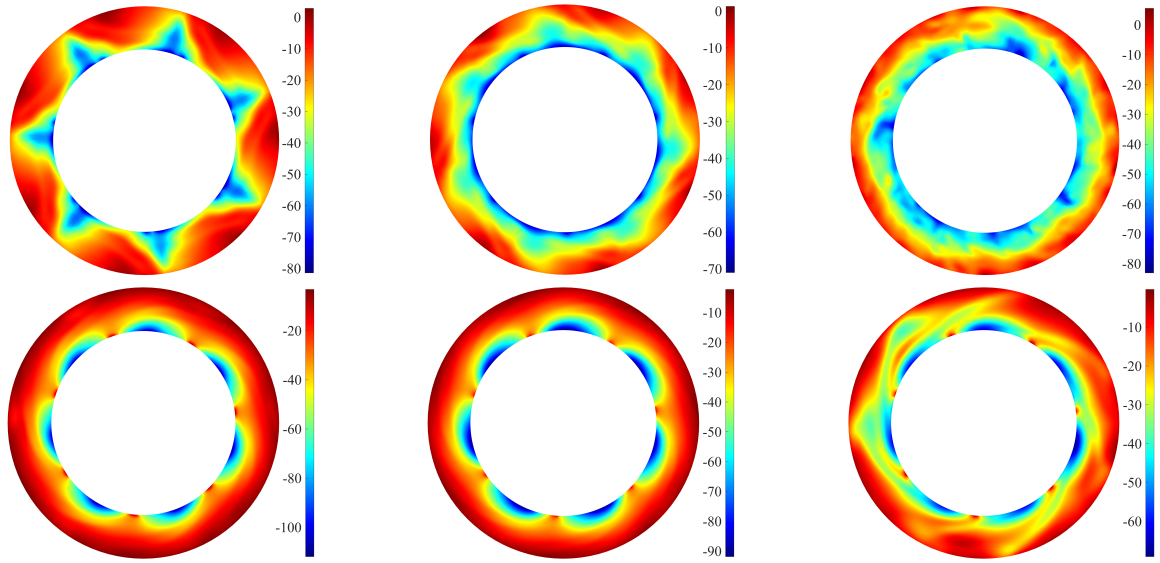


(a) (b) (c)

**Figure 9. Instantaneous color maps of the static pressure $p$ (pa) at the mid-height of the diffuser at the flow rate $0Q/Q_d = 1.00$ obtained by the URANS (top figures) and RANS (bottom figures) for: (a) case A, (b) case B, and (c) case C.**

on fig. 6 (a). The corresponding flow rate increment, obtained by the numerical simulations in the vaneless diffuser, is due to the leakage caused by the pressure difference between the diffuser inlet and the atmospheric pressure. Fig. 7 gives the estimated leakage flow rate ratio that was first obtained from experiments by Heng et al. [9, 10, 11] and the one obtained from CFD. The diffuser performance curves are consequently shifted as plotted on the fig. 6 (b); it shows that simulation results obtained for case C are now in a better agreement with the experimental results.

However at the smallest flow rate, the RANS simulation results are very different compared with the URANS results. This is due to the rotating stall phenomena occurring in the vaneless diffuser that was already detected in previous works. Such an instability cannot be captured properly by the steady calculations. This can be seen on fig. 8 (a), 8 (b)

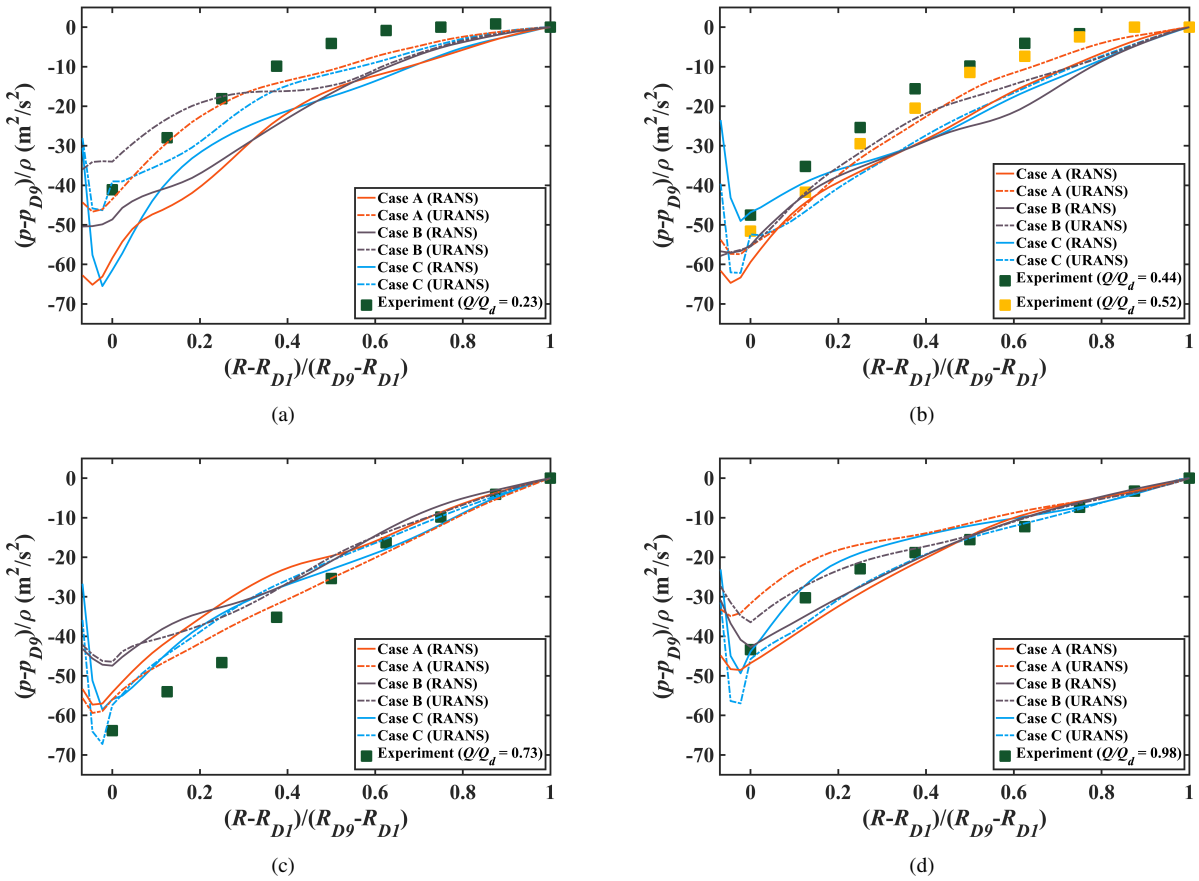


**Figure 10. Diffuser radial pressure recovery distributions for different flow rates. (a)** $Q/Q_d = 0.25$**, (b)** $Q/Q_d = 0.50$**, (c)** $Q/Q_d = 0.75$**, (d)** $Q/Q_d = 1.00$**.**

and 8 (c). They show the static pressure maps at mid height section between hub to shroud obtained by the numerical simulations for $Q/Q_d = 0.25$, using URANS (top figures) and RANS (bottom figures) for each three cases A, B and C respectively. Three stall cells can be observed very clearly in the case A and case B of the URANS results which well corresponds to the PIV study carried out by Dazin in 2011 [8] in previous investigations.

For the cases A and B at the design flow rate $Q/Q_d = 1.00$, the numerical diffuser performance is still very different from the experiment. This is due to another instability developing at the design flow rate and enhancing the impeller wake inside the diffuser (see fig. 9). A peculiar seven-periodic pattern is observed in the vaneless diffuser far from the diffuser inlet for case A and case B looking at the URANS results. Such instability is normally tamed down by the leakage flow in case C, which results in better performance close to design conditions. As the RANS simulations cannot capture the time dependent instability for case A and case B at the design flow rate, they over-predict the diffuser performance.

The radial distributions of the pressure recovery are plotted in fig. 10, for all three configuration cases (A, B and C) at four different flow rates. The non-dimensional radial position equals zero at the first radial location of the experimental wall pressure tap in the vaneless diffuser $D1$. The negative radial value corresponds to the region where strong jet and wake mixture usually occurs just after the impeller outlet section. This is the reason why URANS results can better capture the corresponding large local pressure losses corresponding to negative pressure recovery with large gradients.

For $Q/Q_d = 0.25$ (fig. 10 (a)), the RANS simulation cannot correctly predict the diffuser pressure recovery owing to the rotating stall. As the flow rate increases, for $Q/Q_d = 0.50$ to $Q/Q_d = 0.75$ (respectively fig. 10 (b) and fig. 10 (c)), both URANS and RANS simulation results are a good agreement with the experiments.

At the design flow rate $Q/Q_d = 1.00$ (fig. 10 (d)), an important difference can be observed between the RANS and URANS simulations. This is attributed to the instability development that was previously pointed out in the previous section for case A and B.

## 4. CONCLUSIONS

Performances on a pump model using air as working fluid is numerically and experimentally investigated with a focus on the vaneless diffuser characteristics. Three different geometrical configurations have been tested for the RANS and URANS

simulations for the analysis of the leakage effects and make more precise comparisons with experimental results.

The leakage flow can significantly affect the flow characteristics depending on the volume flow rate at the impeller inlet. The simulation results show little influence of the leakage on the global performance and impeller performance, but show a significant impact on the diffuser behavior.

When correctly taking the local leakage effects into account:

- The comparisons between numerical predictions and experiments are significantly improved. URANS approach is always better than RANS one, mainly for the vaneless diffuser performance analysis.
- For off-design low flow rates, like for $Q/Q_d$ = 0.25, three-stall-cells structures can be observed for the configuration that corresponds to the experimental one. Moreover, a different instability is observed to develop at the design flow rate $Q/Q_d$ = 1.00. A more precise analysis of such a complex phenomenon will be performed in future works.

## ACKNOWLEDGEMENTS

We kindly acknowledge the GENCI (grand équipement national de calcul intensif) for the numerical resources granted to conduct this study under the project A0102A01741. Furthermore, we appreciate the support of the China Scholarship Council for the doctoral students of M. Fan (CSC student number 201908320328).

## REFERENCES

[1] Jansen, W., 1964, "Rotating Stall In a Radial Vaneless Diffuser", *Journal of Basic Engineering-Transactions of the ASME*, Vol. 86(4), pp. 750–758.

[2] Jansen, W., 1964, "Steady Fluid Flow in A Radial Vaneless Diffuser", *Journal of Basic Engineering-Transactions of the ASME*, Vol. 86(3), pp. 607–617.

[3] Senoo, Y., and Kinoshita, Y., 1977, "Influence of Inlet Flow Conditions and Geometries of Centrifugal Vaneless Diffusers on Critical Flow Angle for Reverse Flow", *ASME Journal of Fluids Engineering*, Vol. 99(1), pp. 98–103.

[4] Frigne, P., and Van Den Braembussche, R., 1984, "A Theoretical Model for Rotating Stall In the Vaneless Diffuser of A Centrifugal Compressor", *Journal of Engineering for Gas Turbines and Power*, Vol. 106, pp. 468–474.

[5] Sundström, E., Mihăescu, M., Giachi, M., Belardini, E., and Michelassi, V., 2017, "Analysis of Vaneless Diffuser Stall Instability in A Centrifugal Compressor.", *International Journal of Turbomachinery, Propulsion and Power*, Vol. 2(4), p. 19.

[6] Wuibaut, G., Dupont, P., Caignaert, G., and Stanislas, M., 2000, "Experimental Analysis of Velocities in the Outlet Part of A Radial Flow Pump Impeller and the Vaneless Diffuser using Particle Image Velocimetry", *Proceedings of the XX IAHR Symposium (Charlotte USA)*, Charlotte, USA, pp. 6–9.

[7] Dazin, A., Coutier-Delgosha, O., Dupont, P., Coudert, S., Caignaert, G., and Bois, G., 2008, "Rotating Instability in the Vaneless Diffuser of A Radial Flow Pump", *Journal of Thermal Science*, Vol. 17, pp. 368–374.

[8] Dazin, A., 2011, "High-speed Stereoscopic PIV Study of Rotating Instabilities in A Radial Vaneless Diffuser", *Experiments in Fluids*, Vol. 51, pp. 83–93.

[9] Heng, Y. G., Dazin, A., Ouarzazi, M. N., and Si, Q. R., 2016, "Experimental Study and Theoretical Analysis of the Rotating Stall in a Vaneless Diffuser of Radial Flow Pump", *IOP Conference Series: Earth and Environmental Science*, Vol. 49, p. 032006.

[10] Heng, Y. G., Dazin, A., and Ouarzazi, M. N., 2017, "Linear Stability Analysis of Rotating Stall in A Wide Vaneless Diffuser", *Proceedings of 12th European Conference on Turbomachinery Fluid dynamics & Thermodynamics*, Stockholm, Sweden, Vol. EUROPEAN TURBOMACHINERY SOCIETY, pp. ETC2017–301.

[11] Heng, Y. G., Dazin, A., Ouarzazi, M. N., and Si, Q. R., 2018, "A Study of Rotating Stall in A Vaneless Diffuser of Radial Flow Pump", *Journal of Hydraulic Research*, Vol. 56(4), pp. 494–504.

[12] Dupont, P., Bayeul-Laine, A. C., Dazin, A., and Bois, G., 2014, "Leakage Flow Simulation in A Specific Pump Model", *IOP Conference Series: Earth and Environmental Science*, Montreal, Canada, Vol. 22, pp. 1–10.

[13] Pavesi, G., Dazin, A., Cavazzini, G., Caignaert, G., Bois, G., and Guido, A., 2011, "Experimental and Numerical Investigation of Unforced unsteadiness in a Vaneless Radial Diffuser", *9th european conference on turbomachinery-fluid dynamics and thermodynamics*, Istanbul, Turkey, pp. 625–636.

[14] Kratzsch, C., Timmel, K., Eckert, S., and Schwarze, R., 2015, "URANS Simulation of Continuous Casting Mold Flow: Assessment of Revised Turbulence Models", *Steel Research International*, Vol. 86(4), pp. 400–410.